Extreme Artificial Airglow Induced by HF Pumping Sporadic E Layer at the SURA Facility

Alexander Beletsky * , Ivan Tkachev , Savely Grach , Alexei Shindin , Igor Nasyrov , Denis Kogogin , Valery Emeljanov , Yulia Legostaeva , Elena Tareeva , Sergey Moiseev , Roman Vasilyev

Posted Date: 27 March 2026

doi: 10.20944/preprints202603.2129.v1

Keywords: ionosphere; sporadic E layer; artificial airglow; powerful radio wave; the SURA facility

 doi:10.20944/preprints202603.2129.v1

Article

Extreme Artificial Airglow Induced by HF Pumping Sporadic E Layer at the SURA Facility

Alexander Beletsky [1,*], Ivan Tkachev [1], Savely Grach [2], Alexey Shindin [2], Igor Nasyrov [3], Denis Kogogin [3], Valery Emeljanov [3], Yulia Legostaeva [2], Elena Tareeva [2], Sergey Moiseev [2] and Roman Vasiliev [1]

[1] Institute of Solar–Terrestrial Physics SB RAS, Lermotova Street, 126A, a/b 291, Irkutsk 664033, Russia
[2] Lobachevky State University, Gagarina Avenue, 23, N. Novgorod 603022, Russia
[3] Institute of Physics, Kazan Federal University, Kremlevkaya Street, 16a, Kazan 420008, Russia
* Correspondence: beletsky@iszf.irk.ru

Abstract

The paper presents experimental data on the observation of an artificial airglow of the ionosphere induced by HF pumping by the SURA heating facility during the presence of a blocking sporadic E layer of the ionosphere. Optical observations were carried out on August 5, 2024. using a three-channel photometer and CCD cameras with narrow-band filters. Emission of atomic oxygen at the wavelength λ = 557.7 nm (green line), as well as airglow close to red line of atomic oxygen at λ = 630 nm and band of molecular nitrogen ions $1NGN_2^+(0-0)$ at λ = 391.4 nm (blue band), were recorded. The induced emission intensity in the green line reached $\sim$ 270 R, larger than ever measured. Additional lower-intensity glow spots in the green line southwest and northeast of the main spot ($\sim$12° from zenith), detected by the CCD camera could be due to the side lobes of the SURA antenna pattern. The atypical behavior of the time course of the intensity in the red line with sharp fronts of increase and decrease may indicate the detection of emission lines of hydroxyl groups in the OH(9-3) and OH(5-0) bands, spectrally close to 630 nm. More detailed analysis of the results obtained and new similar experiments will let to understand more deeply processes occurring in the upper atmosphere/lower ionosphere over high solar activity.

Keywords: ionosphere; sporadic E layer; artificial airglow; powerful radio wave; the SURA facility

1. Introduction

Enhancements of the night airglow at different wavelengths, e.g. at λ = 630 nm (transition $O^1D \rightarrow O(^3P)$, red line of the atomic oxygen) λ = 557.7 nm ($O(^1S) \rightarrow O(^1D)$, green line of the atomic oxygen), and λ = 391.4 nm, λ = 427.8 nm (blue lines of the nitrogen ion), due to modification of the F-region ionosphere by powerful high-frequency (HF) radio waves have been studied since early 1970s [1–8]. Such an emission is considered to be evidence that the HF modified electron distribution function is non-Maxwellian because a significant flux of suprathermal electrons is required to produce the artificial airglow. The suprathermal tail is known to develop as a result of the electron acceleration by pump-induced plasma waves.

At the Sura facility (Nizhny Novgorod, Russia), such studies have been conducted since 1983 [7], a set of experiments were carried out with participance of the foreign scientists in the 1990s and 2000s [3,9], and regular observations have been provided since 2006 [10,11]. The brightness of the artificial airglow depends on the conditions of the experiment, such as the pump wave frequency and power, altitude of the pump interaction with ionospheric plasma, geographic position of the heating facility, ionospheric critical frequency etc. E.g., at the HAARP facility in the red and green lines, respectively, the brightnesses can achieve 280 R and 50-70 R [12], while at Arecibo heating facility the brightnesses in the same lines were 50-70 R and $\sim$ 5 R [13]. At the EISCAT heating

 doi:10.20944/preprints202603.2129.v1

facility the brightnesses ∼ 50-70 R in the red line, ∼ 10 R in the green line and ∼ 5 R in the blue line (427.8 nm, $1NGN_2^+(0-1)$) were measured [14]. These values were obtained for the airglow generated in the F-region.

Apart from the experiments described in this study, enhancements of the green line emission during the development of the E_s layers have been observed only few times: at the Arecibo heating facility in January 1998 [15] and at the SURA facility in September 2021 [16] and August 2023 [17]. In the former experiment, 55 R airglow were registered at λ = 557.7 nm. Also, for the first time the emission at (640 - 680 nm (first positive neutral molecular bands of N_2), was observed, as well possible enhancement of the emission in the 710-760 nm range was mentioned. The brightness of the artificial airglow at 557.7 nm generated at the E_s at the SURA reached several Rayleighs [16,17]. Also, at the SURA facility, the E_s-related blue line artificial airglow at λ = 391.4 nm was revealed [17].

In this paper we report results of the experiment performed at the SURA facility on August 5, 2024 when during very long time (about 1.5 hour) existence of the powerful sporadic E layer with blocking frequency more than 9 MHz, the extremely strong artificial airglow at 557.7 nm and noticeable enhancement of the airglow close to 391.4 nm and 630 nm were observed.

Below, in the Section 2 we describe the geophysical conditions of the experiment, experimental equipment and methods used for the data analysis, the Section 3 contains the statement of the experimental results; in the Section 4 the results obtained are discussed. The conclusions are presented in the Section 5.

2. Experimental Equipment and Methods

For pumping ionosphere, we used the SURA facility situated near Nizhny Novgorod, Russia (geographic coordinates 56.13°N, 46.10°E). During the experiment on August 5, 2024, the pump wave of ordinary polarization (O-mode) radiated vertically from 18:48 UT (LT = UT + 3 h) until 23:28 UT in 6-minute cycles: 2.5 minutes of continuous wave emission followed by a 3.5-minute pause. The pump wave frequency f_0 was chosen to be below the critical frequency of the F_2 layer, foF_2. During the time interval considered in the present article, from 19:25 UT till 20:50 UT, f_0 = 5750 kHz was constant. The effective radiated power P_{eff} of the SURA transmitters was ∼ 150 MW throughout the experiment. Ionospheric conditions were monitored using ION-FAST ionosonde [18] located in close proximity to the SURA antenna system.

On August 5, 2024, the geomagnetic field was weakly disturbed. On August 4, a magnetic storm of level G3 (Kp=7) occurred between 12:00 and 18:00 UT [19]. On August 5, the magnetic activity decreased to a quiet level (Kp=3-), but it again reached the threshold of a weak storm of G1 (Kp=5) after 23:00 UT. According to [20] in the time interval 19-21 UT, the Dst index was ≈ -13 (the minimum Dst index on the previous day was -100).

For registration of the airglow the following optical instruments were used at three observation sites.

Directly next to the SURA facility: 3-channel photometer (channels with an interference filter transmission centers 391.4 nm, 557.7 nm, 630 nm with full width at half maximum (FWHM) ∼ 10 nm, temporal resolution 10 ms and fields of view (FoV) ∼ 10°); CCD camera Andor (filter with a transmission center 557.7 nm and FWHM ∼ 10 nm) with ∼ 17° FoV; CCD camera SBig1 with 630 nm interference filter (FWHM ∼ 10 nm, ∼ 15°FoV).

Zakluchnaya observation site (55.36°N, 44.33°E, ∼ 115 km from the SURA facility): similar 630 nm camera SBig2.

Kazan Federal University magnetic observatory (55.56°N, 48.45°E, ∼ 170 km east of the SURA facility): Keo Sentinel optical system designed to record the spatial distribution of the 630 nm emission intensity with the interference filter (FWHM ∼ 2 nm, 145°FoV).

All CCD cameras started acquiring data synchronously at 0 and 30th seconds of each minute with an exposure time 27 s (dead time between frames being 3 s).

Astrometric calibration for cameras with a field of view less than 30 degrees was performed using the Astrometry.net software [21]. Astrometry output data are in the International Celestial

 doi:10.20944/preprints202603.2129.v1

Reference System (ICRS). For the wide-angle cameras, astrometric calibration software based on the work of [22,23] was used. The software output — azimuth and elevation angle for each pixel in the frame — was converted to the ICRS coordinate system using the Astropy module [24]. For the wide-angle KEO Sentinel frames, azimuths and zenith angles were recalculated for the SURA observation point. The recalculation is performed for a selected layer height above the Earth's surface using the Astropy module [24].

The trends caused by natural variations in the nightglow were removed using the method described in the article [16].

3. Experimental Results

Figure 1 illustrates ionospheric conditions of the experiment of 05.08.2024. In the panel (b) the time course of the F-layer critical frequency (foF_2, black points) and the sporadic E layer critical frequency (f_tE_s, violet points) obtained by ION-FAST are shown. Height of the E_s layer of the time interval was $\sim$ 105-110 km. Besides, four ionograms registered by ION-FAST at 19:36 UT, 20:00 UT, 20:12 UT and 20:42 UT are inserted in the panel (a).

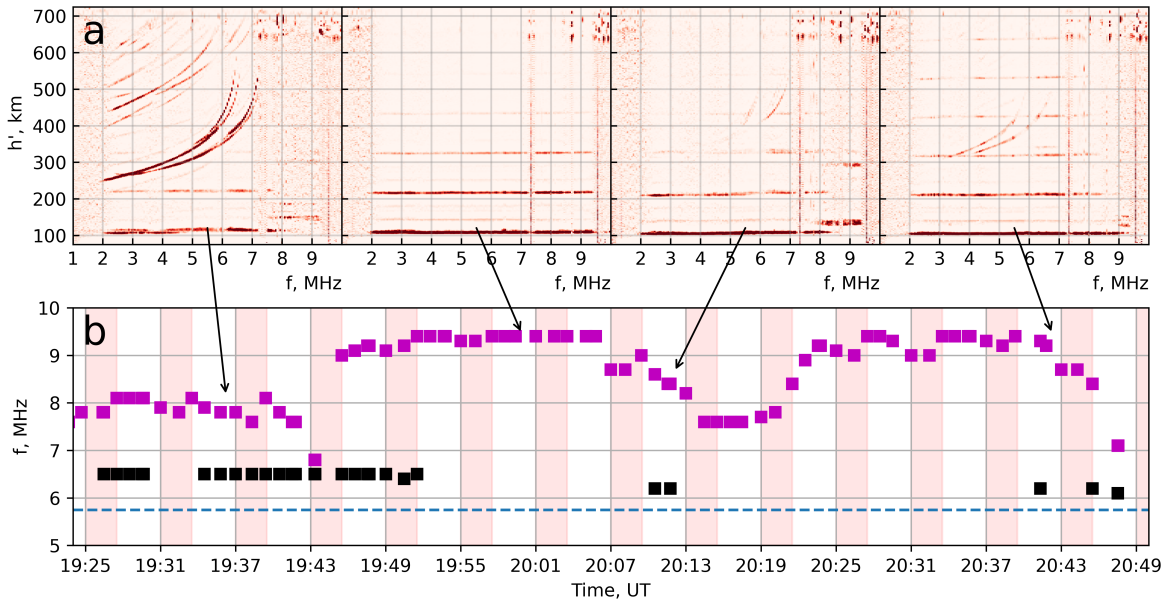

Figure 1. ION-FAST data of f_oF_2 (black), f_tE_s (pink) and pumping frequency f_0 (blue dashed) for August 5, 2024 (panel b). Panel a - ionograms for 19:36, 20:00, 20:12 and 20:42 UT

It is seen, that during the SURA operation at f_0=5.75 MHz two types of the time intervals with different conditions can be highlighted. There are, first, (i) 19:25 UT - 19:31 UT, 19:34 UT - 19:53 UT, 20:10 UT - 20:13 UT and 20:40 UT - 20:49 UT, when translucent E_s with $f_tE_s \sim$ 7.8-8.1 MHz (till 9 MHz) does not block the F-layer totally, which is well seen in the ionograms together with E_s (see Figure 1a). Second, there are intervals (ii) 19:31 UT – 19:34 UT, 19:54 UT- 20:10 UT and 20:14 UT -20:39 UT, when the F-region is totally blocked by the E_s with $f_tE_s \sim$ 9.5 MHz, and the pump wave does not penetrate to the F-layer.

Figure 2 exhibits results of the airglow measurements. Panel (a) shows frames at 557.7 nm registered by the Andor CCD camera for certain time moments indicated by arrows connecting panels (a) and (b). The airglow spots close to the center of the frames are well seen. Additional glow spots, possibly associated with side lobes of the SURA antenna pattern, are also visible on the panel (a). Panels (b)-(e) show the detrended photometric curves for the 557.7 (b), 630 nm (c,d) and 391.4 nm (e) lines obtained by the three-channel photometer (solid noisy lines, panels (b), (c), (e)), as well as by CCD cameras (curves with dots) Andor (panel (b)), SBig1 (panel (c)), and KEO Sentinel (panel (d)). For the KEO Sentinel camera, a transformation of the FoV for the SURA observation point was

 doi:10.20944/preprints202603.2129.v1

performed, taking into account the layer's height above the Earth's surface. All intensity curves for the cameras are calculated as an average over the FoV in the frame indicated by the red dashed circle in the Figure 2a, selected as the region of maximum airglow intensity for the Andor camera. The photometer FoV is shown by the blue dashed circle in the Figure 2a. The pumping schedule is indicated by the colored rectangles.

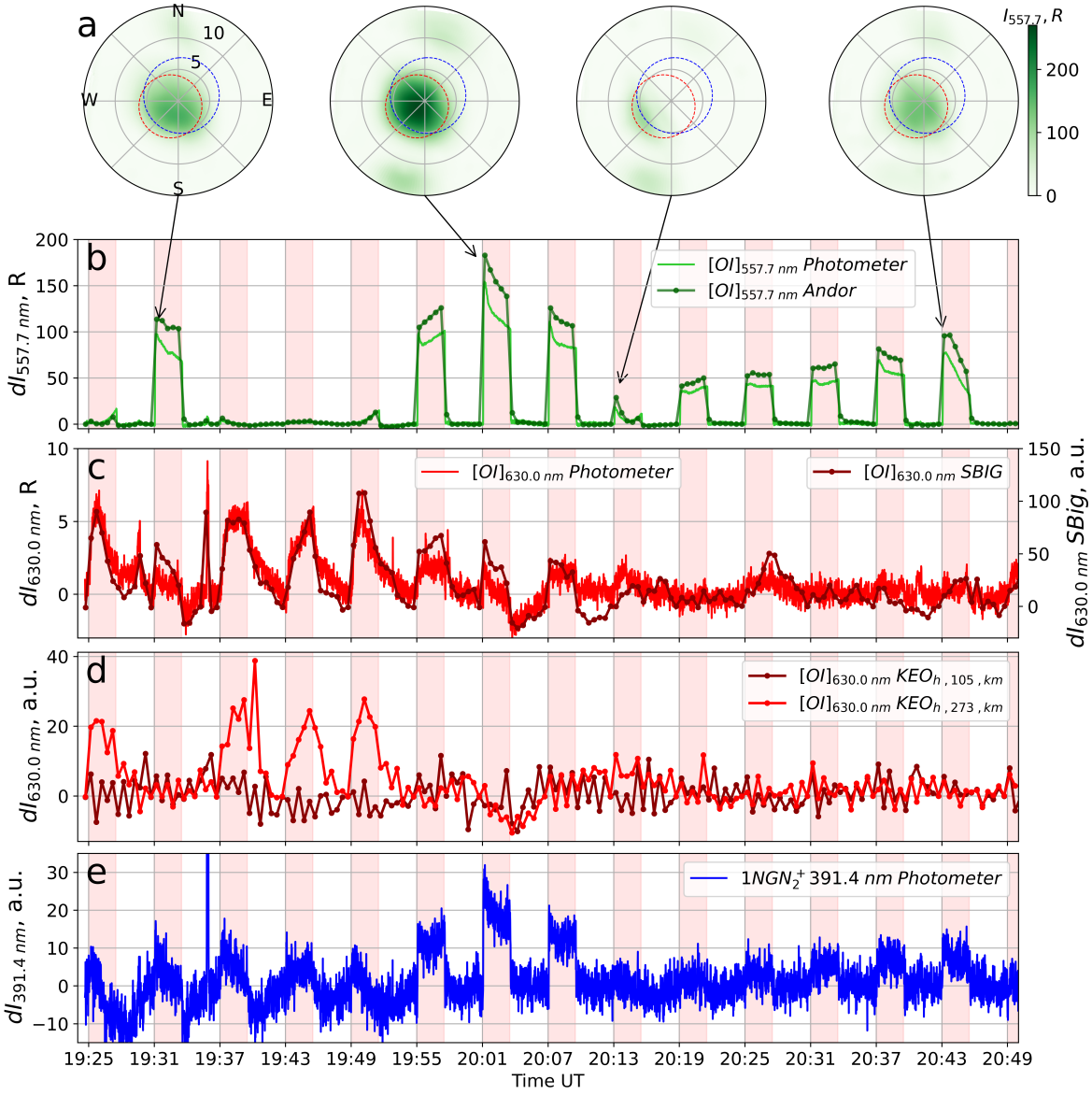

Figure 2. Frames and detrended photometric emission curves on August 5, 2024: (a) Andor camera images (557.7 nm) showing the airglow spots. Dashed circles - photometer FoV (blue) and region of max intensity (red); (b) Time series of 557.7 nm intensity from photometer (light green) and Andor camera (bright green); (c) Same as (b) for 630.0 nm (photometer and SBig1); (d) Keo Sentinel data mapped to 105 km (E_s layer) and 273 km (F_2 layer) altitudes; (e) Photometer data close to 391.4 nm; Red rectangles - pump wave turn on intervals.

According to Figure 2c, the dynamics of the red line (630 nm) airglow in the pumping cycles beginning at 19:25,19:37, 19:43, and 19:49 UT, corresponding to the (i)-intervals (translucent E_s) the intensity exhibits a typical behavior for pumping the F_2 ionospheric layer (slow increasing and decreasing artificial airglow in intensity). Similar, but much weaker red line airglow can be distinguished during the cycle beginning at 20:13 UT, also with the translucent E_s. Using triangulation from the SBig1, SBig2, and KEO Sentinel cameras for cycles with a presence of such typical red line airglow, the altitude of the glow spot observed in these cycles was determined to be $\sim$ 273 km.

 doi:10.20944/preprints202603.2129.v1

Figure 2d displays KEO Sentinel data for the altitudes 273 km and 105 km (the latter corresponds to the E_s altitude). It is seen that the time course of the red line airglow intensity for the F-region altitude (273 km) is similar for the cycles with translucent E_s for SBig1 camera while no increase is observed in the red line at an altitude of 105 km. During these pumping cycles small increase in the green line intensity (about few Rayleigh) can be distinguished (Figure 2b), the pump-induced blue line airglow was also registered (Figure 2e).

Just after the cycles with the translucent E_s, in the three subsequent cycles (19:55, 20:01, and 20:07 UT), during the blocking sporadic E, extremely strong artificial airglow ($\gtrsim$ 100 R) is observed in the green line, the maximum brightness magnitude across the Andor CCD FoV achieves $\sim$ 270 R. Such values never observed in the previous experiments when artificial green line airglow was associated with the sporadic E-layer. In the same time, a noticeable enhancement (up to 2 times) was observed for the blue line intensity. Similar enhancements in the green line brightness of the same order are observed during other cycles with blocking E_s beginning at 19:31, 20:19, 20:25, 20:31 UT, and with translucent E_s in cycles 20:37 and 20:43 UT. Note that during the latter cycle, the E_s and the green line airglow noticeable weakens to the end of the cycle. The pump-induced blue line is also observed during these cycles, but with smaller brightness then during 19:55- 20:10 UT.

Note also, that during the cycle 19:31-19:37 UT as well after 19:55 UT in the data of KEO Sentinel no increase in the intensity of 630 nm emission is observed neither for the F layer heights nor for the sporadic E layer heights of the ionosphere (see Figure 2d). However, the unusual behavior of the red line with short development and decay times were observed in cycles beginning at 19:31, 19:55, 20:01, and 20:07 UT as measured by the photometer ($\sim$ 0.6 s) and SBig1 camera (see Figure 2, panel (c)).

4. Discussion

The HF-pump-induced airglow generated in the F-region of the ionosphere has been studying since the beginning of the ionospheric modification experiments in early 1970th [1]. For the first time the large 557.7 nm emission produced by HF wave-plasma interactions sporadic E layer was observed at the Arecibo heating facility in January 1998 [15]. Later, two successful observations of the green line pump-induced emission were made at the SURA heating facility [16,17]. In the latter experiment [17], the E_s-related blue line artificial airglow was also revealed.

In the experiment of August 5, 2024, we obtained some new results on E_s-related artificial airglow:

1. For the first time at the SURA facility extremely high intensity ($\sim$ 270 R) of the airglow has detected in the 557.7 nm line, associated with HF pumping E_s layer much larger than in previous similar experiments. The emission was observed during existence of the strong blocking E_s as well during half-blocking E_s with critical frequency f_0E_s from 7.8 till 9.5 MHz, the pump wave frequency used was f_0=5.75 MHz. In previous experiments the sporadic E-layer was half-blocking; the maximum brightness of the pump-induced E_s - related airglow achieved 55 R for the pump wave frequency f_0=3.175 MHz and critical frequency $f_OE_s \sim$ 4.5 MHz [15] and $\sim$ 10 R for f_0=4.3 MHz and $f_OE_s \sim$ 7 MHz [16] and $\sim$ 7 R for f_0=5.32 MHz and $f_OE_s \sim$ 5.6 MHz [17]. In parallel with the airglow spot attributed the main lobe of the SURA antenna pattern, two weaker glow spots of lower intensity in the green line in the southwest and northeast directions ($\sim$ 12°zenith angles) corresponded to the side lobes of the antenna pattern were detected.
2. During the cycles with strong green line airglow (19:31, 19:55, 20:01, and 20:07 UT) an unusual temporal behavior of the red line emission with sharp forefront of increase and fast decay after the pump wave switch on/off. (see Figure 2c)
3. Similar to [17], the pump-induced enhancement in the blue band airglow was seen during the E_s existence. The enhancements were observed both for blocking E_s (large brightness, simultaneously with strong green line emission) and for partially blocking E_s, with more moderate brightness, of the same order as in the experiment of [17].

 doi:10.20944/preprints202603.2129.v1

Now it is generally adopted that the enhancement of the airglow brightness in all lines under investigation in this paper is a consequence of the excitation of the ionospheric gases (neutral and ions) by the impact of electrons accelerated by pump wave parametrically induced plasma waves.

The airglow is considered to be evidence that the HF modified electron distribution function is non-Maxwellian because a significant flux of suprathermal electrons is required to produce it. This is confirmed by a number of papers considered theory and computer modeling of electron acceleration, electron ohmic heating, optical emission and additional ionization due to particle energization and comparison of the results with the data of specific experiments [14,25–29]. These papers applied to the F- layer pump-induced phenomena. However, the physical explanation of the observed F-layer phenomena could no considered as totally complete.

Due small amount of the experiments [15–17] the understanding of the observed E_s layer airglow features is quite pure. Particularly, in [15] it is shown that the pump power at the E_s altitude exceeded the threshold of the parametric instabilities; [16] and [30] discussed applications of the obtained results to the diagnostics of the E_s peculiarities (wind velocity, visualizing a horizontal E_s structure). [31] has shown that the ohmic heating is not sufficient to provide the strong enhancement in Arecibo experiment [15].

The most impressive result obtained 5 August, 2024 in our experiment is the extremely large intensity of the green line pump-induced airglow exceeding one obtained at Arecibo by 5 times and one in previous SURA experiments by 25 and 40 times for the pump wave power of the same order. This means, most probably, that obtained large intensity value is determined, first of all, by features of the E_s occurred during our experiment. The most noticeable difference is much larger critical frequency $f_t E_s$ and the long time of the layer existence. It's difficult to suppose the reason of this. The essential point could be mentioned is that the experiment was performed a day after quite strong magnetic storm occurred a day before.

The other point is that in August the Perseid meteor shower takes place, a phenomenon that occurs when the Earth passes through a stream of dust particles left behind by Comet Swift-Tuttle.

Unfortunately, we are not familiar with details of the models of the sporadic layers' appearance at different geophysical conditions, this point should be deeply studied. Notice, that the artificial airglow large amplification was obtained only in the green line, the intensity in the blue line was approximately of the same order as in [17].

For further discussion we us the Figure 3, demonstrates spectral transmittance τ of the optical equipment filters and the natural airglow spectrum in the wavelength interval 370 – 770 nm, borrowed from [32].

The unusual behavior of the red line with sharp rise and fall fronts in intensity in cycles beginning at 19:55, 20:01, and 20:07 UT, as measured by the photometer and SBig1 camera (see Figure 2c), can be due to induced emission in the hydroxyl bands OH(9-3) and OH(5-0). The photometer and SBig1 camera are more efficient in recording these bands than KEO Sentinel, due to their larger FWHM $\sim$ 10 nm (see Figure 3). The KEO Sentinel optical system is equipped with a filter with FWHM $\sim$ 2 nm (see Figure 3).

The detection of hydroxyl emission during the recording of 630 nm emission was repeatedly observed. For example, in the work [33] during observations with a limb instrument LiVHySI (effective spectral bandwidth $\sim$ 22 nm) two distinct layers of airglow near a wavelength of 630 nm were detected. The upper $O(^1D)$ layer covers an altitude range of 200–300 km, and the lower thin OH(9–3) layer is limited to an altitude range of 80–100 km. Airglow of OH and $O(^1D)$ emissions was also recorded during limb measurements by the ISUAL (Imager of Sprites and Upper Atmospheric Lightning) instrument on board the FORMOSAT 2 satellite [34]. The measurements were carried out using a CCD camera at a wavelength of 630 nm with a FWHM of $\sim$ 7 nm.

In [15] artificial airglow in the spectral range of 640-680 nm, as well as an increase of intensity in the spectral range of 710-760 nm during HF pumping E_s layer were noted. The authors associated the former one with the emission of the first positive band of N_2 which required significant electron

 doi:10.20944/preprints202603.2129.v1

fluxes at energies $\geq$ 9 eV. The authors did not associate the increase of intensity in the latter range with specific atmospheric emissions. According to [35], OH(6-1) and OH(7-2) hydroxyl bands also emit in spectral ranges of 640-680 nm and 710-760 nm (see Figure 3). It is possible that the authors of [15] recorded an increase in the intensity namely of these bands.

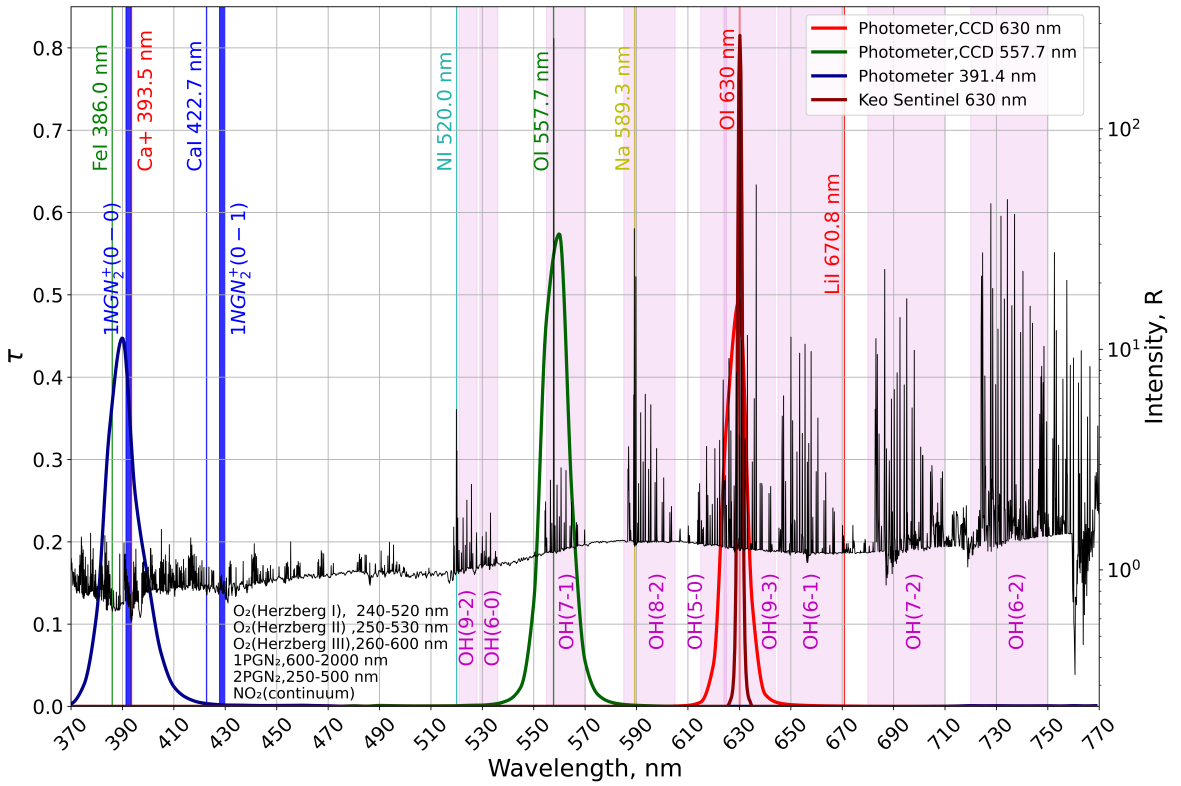

Figure 3. Spectral transmittance τ of the filters and the airglow spectrum at interval 370 - 770 nm

Further, in [36] apparent inconsistencies in the theoretical cross sections and reaction rates were found, indicating that additional measurements of electron-impact excitation of OH are needed. In [37] it is found that the energetic electron precipitation has a small effect on production rate of OH^* excited vibrational states. However, the production rate increases drastically when geomagnetic activity increases. Therefore we conclude that further research into the excitation of OH emission by impact is needed.

The increase in intensity in the blue channel of the 391.4 nm photometer can be due to the following factors:

- Excitation and subsequent emission in the $1NGN_2^+$ band (391.4 nm). This scenario is the most plausible provided that there is a sufficient concentration of N_2^+ is present at the altitude of the E_s layer. The energy required to excite an existing ion N_2^+ from the ground state is $\approx$ 3.17 eV [38]. By electron impact the excited N_2^+ is often formed directly from the neutral N_2. In this case, the energy of N_2 ionization is $\approx$ 15.58 eV [38,39] and it will be summed with the excitation energy. Totally this comprises $\approx$ 18.75 eV.
- Emission of metals FeI 386.0 nm and Ca^+ 393.5 nm, which also fall within the passband of the 391.4 nm photometer filter (see Figure 3) [35]. The excitation energies are 3.2 eV and 3.151 eV, respectively [40].

5. Conclusions

Experimental observations of artificial airglow of the ionosphere at E_s layer altitudes induced by powerful HF radiation from heating facilities are extremely limited. On August 5, 2024, several new features of artificial airglow behavior were obtained:

 doi:10.20944/preprints202603.2129.v1

- For the first time the extreme high intensity ($\sim$ 270 R) of the artificial airglow in the 557.7 nm line, associated with the effect on the E_s layer, has detected at the SURA facility. The detection of additional glow spots of lower intensity in the green line in the southwest and northeast directions from the main spot ($\sim 12^\circ$ zenith angle, see Figure 2a)), may be associated with the side lobes of the SURA antenna pattern.
- The atypical behavior of the red line with sharp fronts of increase and decrease in intensity in the heating cycles according to the photometer and camera SBig1 (see Figure 2c) may be associated with artificial airglow in the hydroxyl bands, presumably OH(9-3) and OH(5-0).
- The intensity increase in the blue channel of the 391.4 nm photometer may be caused by excitation of the $1NGN_2^+$ band (391.4 nm), FeI emission line (386.7 nm), Ca^+ emission line (393.5 nm) or a combination of them.

Author Contributions: Conceptualization, A.B.,S.G. and A.S.; methodology, A.B., I.T., I.N. and D.K.; software, A.B., I.T., V.E., A.S., Y.L. and E.T.; validation, S.G., I.N., D.K. and R.V.; formal analysis, A.B., I.T., V.E., Y.L. and E.T.; investigation, A.B., S.G., I.N. and D.K.; resources, A.S., I.N., D.K. and R.V.; data curation, A.B., I.T., A.S., I.N., D.K., V.E., Y.L., S.M. and E.T.; writing—original draft preparation, A.B. and S.G.; writing—review and editing, S.G., A.B., D.K., and I.N.; visualization, A.B., A.S. and E.T.; supervision, A.B. and S.G.; project administration, A.B., A.S., I.N. and D.K.; funding acquisition, S.G., D.K. and R.V. All authors have read and agreed to the published version of the manuscript.

Funding: The experimental data were obtained by using the Large-Scale Research Facilities (LSRF) «Sura facility» and «Optical instruments» with the financial support from the Russian Science Foundation (RSF) (project No. No 20-12-00197, https://rscf.ru/project/ 20-12-00197) and basic part of the UNN State Assignment FSWR-2023-0038. Data analysis was done with the financial support from the Ministry of Science and Higher Education of the Russian Federation (Subsidy No.075-GZ/C3569/278). Data processing and analysis of the KEO Sentinel optical system was carried out with the financial support of the Russian Science Foundation (project No. 23-77-10029 https://rscf.ru/project/23-77-10029/). Data processing and analysis of the cameras SBig1 and SBig2 were supported by the Russian Science Foundation (project No. 25-72-20019 https://rscf.ru/project/ 25-72-20019/), project supervision was supported by Russian Science Foundation, project no. 25-72-20019.

Institutional Review Board Statement: Not applicable.

Informed Consent Statement: Not applicable.

Data Availability Statement: Dataset available on request from the authors.

Acknowledgments: The authors express their gratitude to the Nizhny Novgorod Scientific Research Radiophysical Institute, the staff of the SURA facility and the head of the Magnetic Observatory of the Kazan Federal University M.P. Cherzor for supporting the experiments.

Conflicts of Interest: The authors declare no conflicts of interest.

Abbreviations

The following abbreviations are used in this manuscript:

CCD	Charge-Coupled Device
EISCAT	European Incoherent Scatter Scientific Association
FoV	Field of View
HAARP	High-frequency Active Auroral Research Program
HF	High Frequency

References

1. Utlaut, W.F.; Cohen, R. Modifying the Ionosphere with Intense Radio Waves. *Science* **1971**, *174*, 245–254. https://doi.org/10.1126/science.174.4006.245.
2. Bernhardt, P.A.; Duncan, L.M.; Tepley, C.A. Artificial Airglow Excited by High-Power Radio Waves. *Science* **1988**, *242*, 1022–1027. https://doi.org/10.1126/science.242.4881.1022.

 doi:10.20944/preprints202603.2129.v1

3. Bernhardt, P.A.; Wong, M.; Huba, J.D.; Fejer, B.G.; Wagner, L.S.; Goldstein, J.A.; Selcher, C.A.; Frolov, V.L.; Sergeev, E.N. Optical remote sensing of the thermosphere with HF pumped artificial airglow. *Journal of Geophysical Research: Space Physics* **2000**, *105*, 10657–10671. https://doi.org/10.1029/1999JA000366.
4. Pedersen, T.R.; Carlson, H.C. First observations of HF heater-produced airglow at the High Frequency Active Auroral Research Program facility: Thermal excitation and spatial structuring. *Radio Science* **2001**, *36*, 1013–1026. https://doi.org/10.1029/2000RS002399.
5. Rietveld, M.T.; Kosch, M.J.; Blagoveshchenskaya, N.F.; Kornienko, V.A.; Leyser, T.B.; Yeoman, T.K. Ionospheric electron heating, optical emissions and striations induced by powerful HF radio waves at high latitudes: Aspect angle dependence. *Journal of Geophysical Research: Space Physics* **2003**, *108*, 1141. https://doi.org/10.1029/2002JA009543.
6. Kvammen, A.; Gustavsson, B.; Sergienko, T.; Brändström, U.; Rietveld, M.; Rexer, T.; Vierinen, J. The 3-D distribution of artificial aurora induced by HF radio waves in the ionosphere. *Journal of Geophysical Research: Space Physics* **2019**, *124*, 7270–7285. https://doi.org/10.1029/2018JA025988.
7. Gumerov, R.I.; Kapkov, V.B.; Komrakov, G.P.; Nasyrov, A.M. Artificial ionospheric glow caused by the short-term effect of high-power RF radiation. *Radiophysics and Quantum Electronics* **1999**, *42*, 463–465. https://doi.org/10.1007/BF02677582.
8. Blagoveshchenskaya, N.F.; Kornienko, V.A.; Borisova, T.D.; Thidé, B.; Kosch, M.J.; Rietveld, M.T.; Mishin, E.V.; Luk'yanova, R.Y.; Troshichev, O.A. Ionospheric HF pump wave triggering of local auroral activation. *Journal of Geophysical Research: Space Physics* **2001**, *106*, 29071–29089, [https://agupubs.onlinelibrary.wiley.com/doi/pdf/10.1029/2001JA900002]. https://doi.org/https://doi.org/10.1029/2001JA900002.
9. Grach, S.M.; Kosch, M.J.; Yashnov, V.A.; Sergeev, E.N.; Atroshenko, M.A.; Kotik, P.V.; Stepanyuk, S.V.; Shindin, A.V. On the location and structure of the artificial 630-nm airglow patch over Sura facility. *Annales Geophysicae* **2007**, *25*, 689–700. https://doi.org/10.5194/angeo-25-689-2007.
10. Grach, S.M.; Klimenko, V.V.; Shindin, A.V.; Nasyrov, A.M.; Sagdeev, R.Z.; Karashtin, A.N.; Grigorev, G.I. Airglow during ionospheric modifications by the Sura facility radiation. Experimental results obtained in 2010. *Radiophysics and Quantum Electronics* **2012**, *55*, 33–50. https://doi.org/10.1007/s11141-012-9347-3.
11. Shindin, A.; Grach, S.; Klimenko, V.; Nasyrov, I.; Sergeev, E.; Beletsky, A.; Taschilin, M.; Gumerov, R. The 630 nm and 557.7 nm Airglow During HF Ionosphere Pumping by the SURA Facility Radiation for Pump Frequencies Near the Fourth Electron Gyroharmonic. *Radiophysics and Quantum Electronics* **2015**, *57*. https://doi.org/10.1007/s11141-015-9562-9.
12. Djuth, F.T.; Pedersen, T.R.; Gerken, E.A.; Bernhardt, P.A.; Selcher, C.A.; Bristow, W.A.; Kosch, M.J. Ionospheric Modification at Twice the Electron Cyclotron Frequency. *Phys. Rev. Lett.* **2005**, *94*, 125001. https://doi.org/10.1103/PhysRevLett.94.125001.
13. Bernhardt, P.A.; Tepley, C.A.; Duncan, L.M. Airglow enhancements associated with plasma cavities formed during ionospheric heating experiments. *Journal of Geophysical Research: Space Physics* **1989**, *94*, 9071–9092. https://doi.org/10.1029/JA094iA07p09071.
14. Gustavsson, B.; Sergienko, T.; Kosch, M.J.; Rietveld, M.T.; Brändström, B.U.E.; Leyser, T.B.; Isham, B.; Gallop, P.; Aso, T.; Ejiri, M.; et al. The electron energy distribution during HF pumping, a picture painted with all colors. *Annales Geophysicae* **2005**, *23*, 1747–1754. https://doi.org/10.5194/angeo-23-1747-2005.
15. Djuth, F.; Bernhardt, P.; Tepley, C.; Gardner, J.; Kelley, M.; Broadfoot, A.; Kagan, L.; Sulzer, M.; Elder, J.; Selcher, C.; et al. Large airglow enhancements produced via wave-plasma interactions in sporadic E. *Geophysical Research Letters* **1999**, *26*, 1557 – 1560. https://doi.org/10.1029/1999GL900296.
16. Beletsky, A.B.; Tkachev, I.D.; Nasyrov, I.A.; Grach, S.M.; Kogogin, D.A.; Shindin, A.V.; Vasilyev, R.V. Some Results of Photometric Measurements of Ionospheric Artificial Airglow at 557.7 and 630 nm Lines of Atomic Oxygen Caused by High-Frequency Radio Emission of the SURA Facility during Development of Sporadic E Layer. *Atmosphere* **2022**, *13*. https://doi.org/10.3390/atmos13111794.
17. Tkachev, I.D.; Beletsky, A.B.; Grach, S.M.; Nasyrov, I.A.; Shindin, A.V.; Kogogin, D.A. Artificial Optical Luminescence of the Ionosphere in the 557.7 nm and 391.4 nm Lines Stimulated by Short-Wave Radio Emission from the Sura Facility. *Radiophysics and Quantum Electronics* **2025**, *67*, 732–739. https://doi.org/10.1007/s11141-025-10414-2.
18. Moiseev, S.P.; Shindin, A.V.; Grekhneva, K.K.; Pavlova, V.A.; Timukin, N.S. ION-FAST as the NIRFIs Ionospheric Diagnostic Platform. *Atmosphere* **2024**, *15*. https://doi.org/10.3390/atmos15020188.

 doi:10.20944/preprints202603.2129.v1

19. Matzka, J.; Stolle, C.; Yamazaki, Y.; Bronkalla, O.; Morschhauser, A. The Geomagnetic Kp Index and Derived Indices of Geomagnetic Activity. *Space Weather* **2021**, *19*, e2020SW002641. https://doi.org/10.1029/2020SW002641.
20. World Data Center for Geomagnetism, Kyoto.; Nose, M.; Iyemori, T.; Sugiura, M.; Kamei, T.; Matsuoka, A.; Imajo, S.; Kotani, T. Geomagnetic Dst index. https://wdc.kugi.kyoto-u.ac.jp, 2015. Accessed: 2024-05-21, https://doi.org/10.17593/14515-74000.
21. Lang, D.; Hogg, D.W.; Mierle, K.; Blanton, M.; Roweis, S. Astrometry.net: Blind Astrometric Calibration of Arbitrary Astronomical Images. *The Astronomical Journal* **2010**, *139*, 1782–1800. https://doi.org/10.1088/0004-6256/139/5/1782.
22. Syrenova, T.; Beletsky, A.; Vasilyev, R. Geo-Referencing Images of Wide-Angle Optical Systems. *Technical Physics* **2024**, *69*, 424–430. https://doi.org/10.1134/S1063784224010407.
23. Barghini, D.; Gardiol, D.; Carbognani, A.; Mancuso, S. Astrometric calibration for all-sky cameras revisited. *Astronomy & Astrophysics* **2019**, *626*, A105. https://doi.org/10.1051/0004-6361/201935580.
24. Astropy Collaboration.; Robitaille, T.P.; Tollerud, E.J.; et al.. The Astropy Project: Sustaining and Growing a Community-oriented Open-source Project and Package for Astronomy. *The Astrophysical Journal* **2022**, *935*, 167. https://doi.org/10.3847/1538-4357/ac7c74.
25. Carlson, H.; Wickwar, V.; Mantas, G. Observations of fluxes of suprathermal electrons accelerated by HF excited instabilities. *Journal of Atmospheric and Terrestrial Physics* **1982**, *44*, 1089–1100.
26. Klimenko, V.; Grach, S.; Sergeev, E.; Shindin, A. Features of the Ionospheric Artificial Airglowcaused by Ohmic Heating and Plasma Turbulence-Accelerated Electrons Induced by HF Pumping of the Sura Heating Facility. *Radiophysics and Quantum Electronics* **2017**. https://doi.org/10.1007/s11141-017-9812-0.
27. Sergienko, T.; Gustavsson, B.; Brändström, U.; Axelsson, K. Modelling of optical emissions enhanced by the HF pumping of the ionospheric F-region. *Annales Geophysicae* **2012**, *30*, 885–895. https://doi.org/10.5194/angeo-30-885-2012.
28. Grach, S.M.; Mityakov, N.A.; Trakhtengerts, V.Y. Electron acceleration in the presence of parametric heating of a bounded layer of plasma. *Radiophysics and Quantum Electronics* **1984**, *27*, 766–770. https://doi.org/10.1007/BF01041384.
29. Grach, S.M.; Mitiakov, N.A.; Trakhtengerts, V.I. Electron acceleration and additional ionization during parametric plasma heating. *Fizika plazmy* **1986**, *12*, 693–701.
30. Kagan, L.; Kelley, M.; Garcia, F.; Bernhardt, P.; Djuth, F.; Sulzer, M.; Tepley, C. Structure of electromagnetic wave induced 557.7 nm emission associated with a sporadic E event over Arecibo. *Physical Review Letters* **2000**, *85*, 218 – 221. https://doi.org/10.1103/PhysRevLett.85.218.
31. Birba, M.; Georgiou, I.; Prokopiou, I.; Veldes, G. Ionosphere thermal response to a HF radio wave interaction, during artificial 5577 Å airglow enhancements at a sporadic E layer. *Physica Scripta* **2025**, *100*. https://doi.org/10.1088/1402-4896/ae0f60.
32. Noll, S.; Kausch, W.; Barden, M.; Jones, A.M.; Szyszka, C.; Kimeswenger, S.; Vinther, J. An atmospheric radiation model for Cerro Paranal. I. The optical spectral range. *Astronomy and Astrophysics* **2012**, *543*, A92, [arXiv:astro-ph.IM/1205.2003]. https://doi.org/10.1051/0004-6361/201219040.
33. Bisht, R.S.; Thapa, N.; Babu, P.N. Enhanced 630nm equatorial airglow emission observed by Limb Viewing Hyper Spectral Imager (LiVHySI) onboard YOUTHSAT-1. In Proceedings of the Multispectral, Hyperspectral, and Ultraspectral Remote Sensing Technology, Techniques and Applications VI; Larar, A.M.; Chauhan, P.; Suzuki, M.; Wang, J., Eds. International Society for Optics and Photonics, SPIE, 2016, Vol. 9880, p. 98801E. https://doi.org/10.1117/12.2223567.
34. Nee, J.B.; Tsai, S.D.; Peng, T.H.; Hsu, R.R.; Chen, A.B.C.; Zhang, S.P.; Huang, T.Y.; Rajesh, P.K.; Liu, J.Y.; Frey, H.U.; et al. OH Airglow and Equatorial Variations Observed by ISUAL Instrument on Board the FORMOSAT 2 Satellite. *Terrestrial, Atmospheric and Oceanic Sciences* **2010**, *21*, 985–995.
35. Khomich, V.; Semenov, A.; Shefov, N. *Airglow as an Indicator of Upper Atmospheric Structure and Dynamics*; Springer Berlin Heidelberg, 2008.
36. Campbell, L.; Brunger, M.J. Electron-impact vibrational excitation of the hydroxyl radical in the nighttime upper atmosphere. *Planetary and Space Science* **2018**, *151*, 11–18. https://doi.org/https://doi.org/10.1016/j.pss.2017.10.010.
37. Ferdi, M.A.; Djebli, M. Analysis of nighttime OH vibrational excited states production rate. *Journal of Atmospheric and Solar-Terrestrial Physics* **2021**, *212*, 105519. https://doi.org/https://doi.org/10.1016/j.jastp.2020.105519.

 doi:10.20944/preprints202603.2129.v1

38. Itikawa, Y. Cross Sections for Electron Collisions with Nitrogen Molecules. *Journal of Physical and Chemical Reference Data* **2006**, *35*, 31–53. https://doi.org/10.1063/1.1937426.
39. Song, M.Y.; Cho, H.; Karwasz, G.P.; Kokoouline, V.; Tennyson, J. Cross Sections for Electron Collisions with N2, N2*, and N2+. *Journal of Physical and Chemical Reference Data* **2023**, *52*, 023104, [https://pubs.aip.org/aip/jpr/article-pdf/doi/10.1063/5.0150618/18025935/023104_1_5.0150618.pdf]. https://doi.org/10.1063/5.0150618.
40. Kramida, A.; Yu. Ralchenko.; Reader, J.; and NIST ASD Team. NIST Atomic Spectra Database (ver. 5.12), [Online]. Available: https://physics.nist.gov/asd [2016, January 31]. National Institute of Standards and Technology, Gaithersburg, MD., 2024.